2021 American Control Conference (ACC)
New Orleans, USA, May 25-28, 2021

Proper Orthogonal Decomposition Reduced Order Model for Tear Film Flows

Samir Sahyoun, Dan Wilson, Seddik M. Djouadi, Steven M. Wise, Hamid Ait Abderrahmane.

***Abstract*— Tear film plays a key role in protecting the cornea surface against contaminations and dry eye syndrome which can lead to symptoms of discomfort, visual trouble, and tear film instability with the potential to damage the ocular surface. In this paper, coupled nonlinear partial differential equations of the fourth order proposed by Aydemir et al. to describe the evolution of tear film dynamics are considered. These equations are of Benney type and known to suffer from unbounded behavior and lack of a global attractor. The objective here is to identify a reduced order modeling framework with the potential to be used as a basis for control in future work using smart tears with a surfactant that can modify the surface tension to prevent tear film breakup. Since the dynamics are infinite dimensional and nonlinear, a reduced order model based on the proper orthogonal decomposition (POD) is developed, analyzed, and compared to the full order model. Numerical simulations illustrate that only a small number of POD modes are required to accurately capture the tear film dynamics allowing for the full partial differential model to be represented as a low-dimensional set of coupled ordinary differential equations.**

I. INTRODUCTION

Tear film, as shown in figure (1), is a thin multicomponent fluid that coats the ocular surface after each blink, a period during which the eye remains open [1]. During the interblink period, which lasts approximately 5 to 10 seconds, the tear film protects the cornea surface from contamination, keeps the eye moist, provides a high-quality optical surface, cleans the eye of foreign bodies, and lubricates the gap between the eyelids and the cornea. During this period, the tear film thins and eventually breaks leading to the formation of dry spots over the surface of the cornea, around which, saltiness (osmolarity) increases. This causes irritation of the cornea, sensation of discomfort, persistent headaches, watering of the eyes and blurred vision. These are considered as symptoms of a common wide spread disease condition, known as dry-eye syndrome[2]. Dry eye syndrome (DES) is a worldwide growing ophthalmological concern [3]. Nowadays, DES does not affect only elder persons, but also affects children because the prolonged exposure to the screens of the electronics devices such as smart phones, tablets and computers. The chances that tear film breaks become higher, when blinking frequency decreases [4].

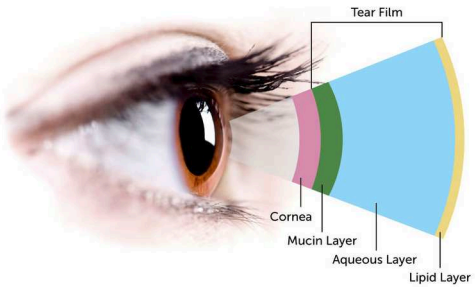

Fig. 1. Tear film layers (Image from [5])

The need for understanding DES from a fluid dynamics perspective gave rise to a growing interest in the problem of tear film dynamics. A variety of investigations dealing with evaporation, gravity, viscosity and surface tension effects are conducted in [6], [7], [8], [9]. Almost all proposed models were developed based on lubrication theory. The first proposed models are typically one-dimensional nonlinear partial differential equation for the thickness of the aqueous layer where gravitational and evaporative effects are added to the single-layer model of the tear film dynamics [10], [11], [8]. The one-dimensional models were solved within time dependent domains, where the lower eyelid is assumed to be stationary while the upper eyelid is moving [12], [13]. The lubrications models were used for instance to investigate the effect of the velocity of the eyelid and the nonuniform surface tension on the stability of the tear layer. The lubrication models were improved by considering a realistic eyelid motion and including effects of the variation of the concentration of the lipid layer above the aqueous one. The evolution of the lipid concentration is also described by a non-linear partial differential equation coupled to the evolution of the film thickness equation [7], [14]. The system of two coupled PDEs was solved in moving domain on flat substrate. This approximation is justified since the tear film's thickness, which is of the order of a few microns, is very small compared to the average radius of curvature of the cornea surface, which is of the order of a centimeter [15].

In this paper, we rely on the success of mathematical models in explaining the thinning mechanism of the tear film and their breakup on the ocular surface. In particular, we are interested in extending the study of Aydemir *et al.* [7] by considering the perspective of designing of smart artificial tears. The idea here is to explore the possibility of controlling

Samir Sahyoun is with the Department of Electrical Engineering, Uppsala University, Sweden. samir1323@gmail.com

Seddik M. Djouadi and Dan Wilson are with the Department of Electrical Engineering and Computer Science, University of Tennessee, Knoxville, Tennessee 37996 USA. djouadi@eecs.utk.edu, dwilso81@utk.edu

Steven M. Wise is with the Department of Mathematics, The University of Tennessee, Knoxville, TN 37996 USA. swise@math.utk.edu

Hamid Ait Abderrahmane is with the Department of Mechanical Engineering, Khalifa University, Abu Dhabi, UAE hamid.abderrahmane@ku.ac.ae

the film thickness of the tear film during the inert blink period using an optimal initial lipid function. To do so we are first using a model reduction approach based on the Proper Orthogonal Decomposition (POD).

POD is a model reduction technique with proven efficient when used to reduce models that approximate nonlinear infinite dimensional systems by high order finite dimensional systems, especially those who describe the dynamics of fluid flows [16], [17], [18].

The remainder of the paper proceeds as follows. In section II the PDE model of the tear film dynamics is described and solved numerically. In section III the POD method is applied and POD modes are extracted. In section IV the reduced order system is computed using Galerkin projection, finally section V includes the conclusions and future work.

II. Tear Film Dynamics

The model that describes the effect of polar lipids, naturally excreted by glands in the eyelid, on the evolution of a pre-corneal tear film is governed by a two coupled nonlinear partial differential equations for the film thickness h and the concentration of lipid Γ, given by the following non-dimensionalized form [7]:

$$h_t = \frac{1}{2}\mathcal{M}(h^2\Gamma_x)_x - \frac{1}{3}\mathcal{C}(h^3(h_{xxx}-\mathcal{B}))_x \quad (1)$$

$$\Gamma_t = \frac{1}{2}\mathcal{M}(h\Gamma\Gamma_x)_x - \frac{1}{2}\mathcal{C}(h^2\Gamma(h_{xxx}-\mathcal{B}))_x \quad (2)$$

where $0 \le x \le L(t)$ is the spacial domain assuming the lower eyelid is stationary at $x=0$ and the upper eyelid is moving with position $x=L(t)$ and speed $L_t(t)$. $\mathcal{M}$ is the Marangoni number, $\mathcal{C}$ is the capillary number, and $\mathcal{B}$ is a Bond number. The initial conditions at $t=0$ are given by $h=\mathcal{H}$ and $\Gamma=1$, where boundary conditions at $x=0$ are:

$$h=\mathcal{H}, \quad \Gamma_x=0, \quad h_{xxx}=\mathcal{B},$$

while boundary conditions at $x=L(t)$ are:

$$h=\mathcal{H}, \quad \Gamma_x=\frac{2L_t}{\mathcal{M}\mathcal{H}}, \quad h_{xxx}=\mathcal{B}+\frac{6L_t}{\mathcal{C}\mathcal{H}}.$$

Expressions for $L(t)$ and $L_t(t)$ used in this paper are taken from [7] and their profiles are shown in figure (2).

The challenge in solving the coupled system (1) and (2) numerically is the moving boundary for the upper eyelid. As done in [19], [20], [21] and others, a change of variables $x \to \frac{x}{L(t)}$ and $h \to \frac{h}{\mathcal{H}}$ is performed such that the coupled system (1) and (2) is transformed into the following equivalent fixed boundary system:

$$h_t = \frac{\mathcal{M}\mathcal{H}}{2L^2}(h^2\Gamma_x)_x - \frac{\mathcal{C}\mathcal{H}^2}{3L}\left(h^3\left(\frac{\mathcal{H}}{L^3}h_{xxx}-\mathcal{B}\right)\right)_x + x\frac{L_t}{L}h_x \quad (3)$$

$$\Gamma_t = \frac{\mathcal{M}\mathcal{H}}{L^2}(h\Gamma\Gamma_x)_x - \frac{\mathcal{C}\mathcal{H}^2}{2L}\left(h^2\Gamma\left(\frac{\mathcal{H}}{L^3}h_{xxx}-\mathcal{B}\right)\right)_x + x\frac{L_t}{L}\Gamma_x \quad (4)$$

in which the spacial domain is now $0 \le x \le 1$ and initial conditions at $t=0$ become $h=1$ and $\Gamma=1$ where boundary conditions at $x=0$ become:

$$h=1, \quad \Gamma_x=0, \quad h_{xxx}=\frac{L^3}{\mathcal{H}}\mathcal{B},$$

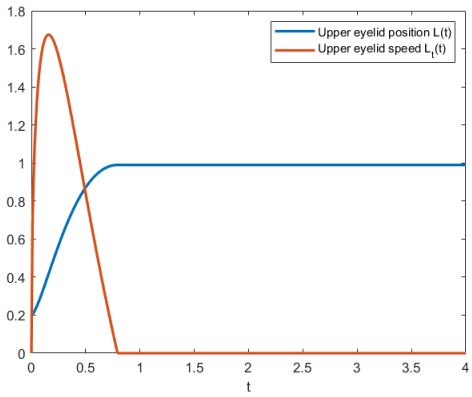

Fig. 2. Upper eyelid normalized position and speed profiles. The eye is closed at $L=0.2$ and fully open at $L=1$

while boundary conditions at $x=1$ become:

$$h=1, \quad \Gamma_x=\frac{2LL_t}{\mathcal{M}\mathcal{H}}, \quad h_{xxx}=\frac{L^3}{\mathcal{H}}\left(\mathcal{B}+\frac{6L_t}{\mathcal{C}\mathcal{H}^2}\right).$$

The transformed system (3) and (4) is solved numerically using finite difference with cell-edge and cell-center points (see Appendix A), with parameters $\mathcal{H}=100$, $\mathcal{C}=7.87\times10^{-7}$, $\mathcal{B}=2.18\times10^{4}$, $\mathcal{M}=1.75\times10^{-2}$, then solution is transformed back to the original form in (1) and (2). Figures 3, 4 and 5 show the film thickness solution and figures (6), (7) and (8) show the lipid concentration for different time stages.

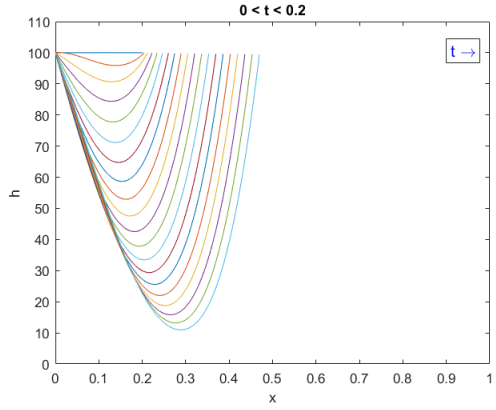

Fig. 3. Film thickness h, early stage

III. POD Basis Computation

Let the solution to (1) and (2) be represented by a linear combination of space dependent basis functions and temporal coefficients as follows:

$$h(x,t) = \sum_{i=1}^{\infty} \alpha_i^h(t)\phi_i^h(x) \quad (5)$$

$$\Gamma(x,t) = \sum_{i=1}^{\infty} \alpha_i^\Gamma(t)\phi_i^\Gamma(x) \quad (6)$$

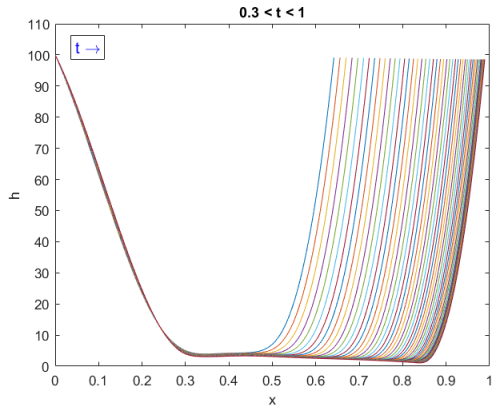

Fig. 4. Film thickness h, mid stage

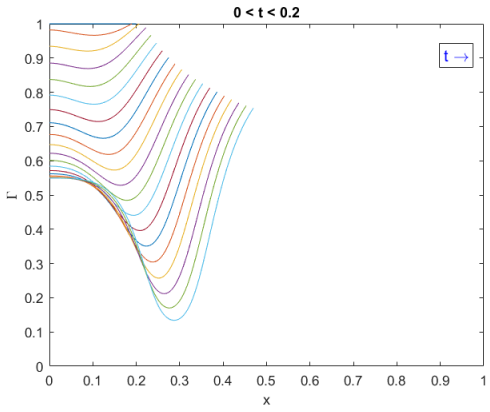

Fig. 6. Lipid Concentration Γ, early stage

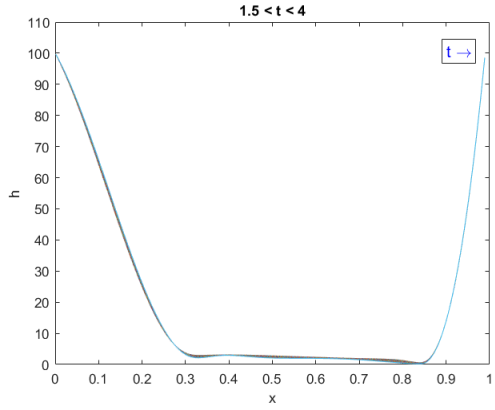

Fig. 5. Film thickness h, late stage

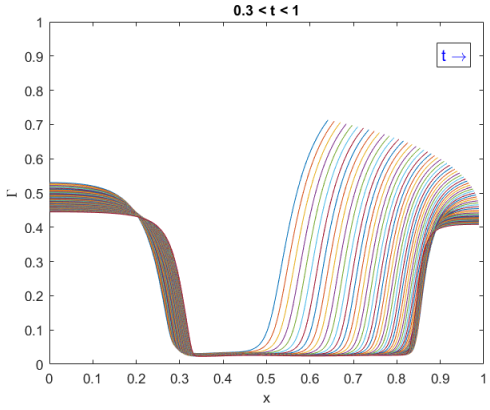

Fig. 7. Lipid Concentration Γ, mid stage

The equalities above are understood to be in the $L^2(\Omega,[0,T))$-sense, i.e.,

$$\lim_{n\to\infty}\int_0^t\int_\Omega |h(x,t)-\sum_{i=1}^{n}\alpha_i^h(t)\phi_i^h(x)|^2dxdt=0 \tag{7}$$

Let R be the desired reduced order then (5) and (6) can be approximated by:

$$h_R(x,t):=\sum_{i=1}^{R}\alpha_i^h(t)\phi_i^h(x) \tag{8}$$

$$\Gamma_R(x,t):=\sum_{i=1}^{R}\alpha_i^\Gamma(t)\phi_i^\Gamma(x) \tag{9}$$

POD provides an optimal set of basis functions such that a low dimensional subspace is obtained by the basis functions projection on the governing coupled PDE system in (1) and (2). The fundamental idea behind POD is as follows: Given the functions $h(x,t)$ and $\Gamma(x,t)$ in the standard Hilbert space $L^2(\Omega,[0,T))$ where $x\in\Omega$ and T is a finite time interval, the R POD basis functions $\{\phi_i^h\}_{i=1}^R$ and $\{\phi_i^\Gamma\}_{i=1}^R$ are computed by minimizing the following cost functions:

$$J(\phi^h):=\int_0^T\int_\Omega \|h(x,t)-\sum_{i=1}^{R}\alpha_i^h(t)\phi_i^h(x)\|^2dxdt \tag{10}$$

$$J(\phi^\Gamma):=\int_0^T\int_\Omega \|\Gamma(x,t)-\sum_{i=1}^{R}\alpha_i^\Gamma(t)\phi_i^\Gamma(x)\|^2dxdt \tag{11}$$

where $h(x,t)$ and $\Gamma(x,t)$ are the solution of the governing coupled PDE system in (1) and (2).
The constrained orthogonality condition for (10) and (11) is:

$$(\phi_i,\phi_j)=\int_\Omega \phi_i\phi_j dx=\delta_{i=j} \tag{12}$$

where $(,)$ is the inner product in $L_2(\Omega)$ and $\delta_{i=j}=1$ if $i=j$ and zero otherwise.
Since no explicit solutions are known for the PDEs (3) and (4) numerical solution snapshots obtained are used at N different times as entries in the snapshots matrices $\{S_i^h\}_{i=1}^N$ and $\{S_i^\Gamma\}_{i=1}^N$. The optimization problem becomes then discrete as follows:

$$J(\phi^h):=\sum_k\sum_m |S^h(x_m,t_k)-\sum_{i=1}^{R}\alpha_i^h(t_k)\phi_i^h(x_m)|^2 \tag{13}$$

$$J(\phi^\Gamma):=\sum_k\sum_m |S^\Gamma(x_m,t_k)-\sum_{i=1}^{R}\alpha_i^\Gamma(t_k)\phi_i^\Gamma(x_m)|^2 \tag{14}$$

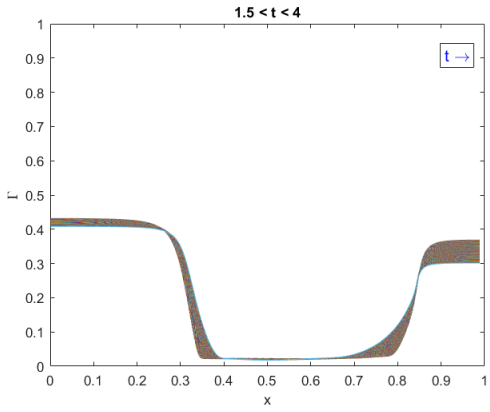

Fig. 8. Lipid Concentration Γ, late stage

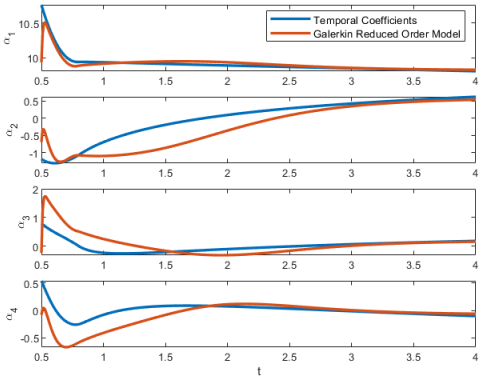

Fig. 10. Reduced order system states

Both (13) and (14) optimization problems have the discrete orthogonality constraints $\phi^{h^*}\phi^h = I_R$ and $\phi^{\Gamma^*}\phi^\Gamma = I_R$, respectively and the subscript $*$ denotes the complex transpose. Solutions are given by the R eigenvectors that correspond to the largest R eigenvalues in the eigenvalue problems [16]:

$$S^h S^{h^*}\phi^h = \lambda^h \phi^h. \tag{15}$$

$$S^\Gamma S^{\Gamma^*}\phi^\Gamma = \lambda^\Gamma \phi^\Gamma. \tag{16}$$

The first 4 POD modes for h are shown in figure (9).

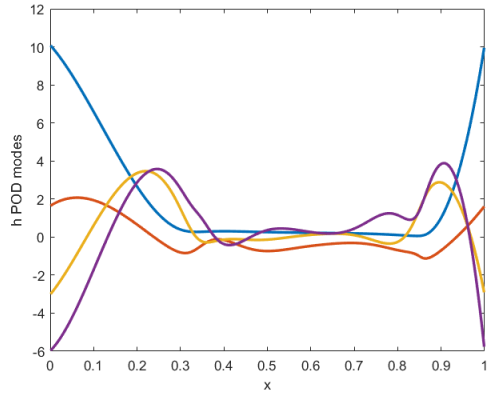

Fig. 9. First 4 POD modes for h

IV. Reduced order system by Galerkin Projection

Galerkin projection is done by performing the inner product defined in (12) for both sides of the PDEs in (3) and (4) with the j^{th} basis functions $\phi_j^h(x)$ and $\phi_j^\Gamma(x)$ (see Appendix B for details). The result is the reduced order system of size R that describe how the POD modes evolve in time. The reduced order system becomes:

$$\begin{aligned} \dot{\alpha} &= f(\alpha) \\ \alpha(0) &= \alpha_0. \end{aligned} \tag{17}$$

where the initial condition in (3) and (4) is projected onto the POD basis to find the initial values α_0. Full expression of $f(\alpha)$ is shown in Appendix B. Since the POD modes are orthogonal, it is easy to find the temporal coefficients in (8) and (9) and use them to validate the reduced order system accuracy in capturing the true dynamics of the full order system. The states of the Galerkin reduced order system of size 4 is shown in figure (10) where it is shown that the reduced order system shows acceptable agreement with the full order system as time evolves. Both h and Γ for the reduced order system compared to the full order system are shown at different times in figures (11), (12), (13) and (14). Results are promising. With a small number of states (we used 4 in our numerical example), we obtained a reduced order system that accurately captures the full order system dynamics. This is important since it is very difficult to control the PDE system in its infinite dimensional form while control theories are well developed for finite dimensional systems.

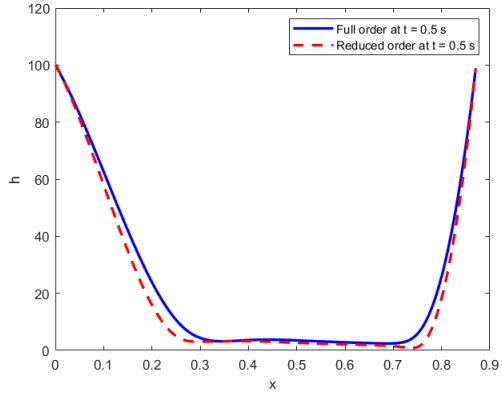

Fig. 11. Tear film thickness, full Vs reduced order systems at $t = 0.5$.

V. Conclusions

In this paper, Benney-type coupled nonlinear partial differential equations of the fourth order governing the evolution of

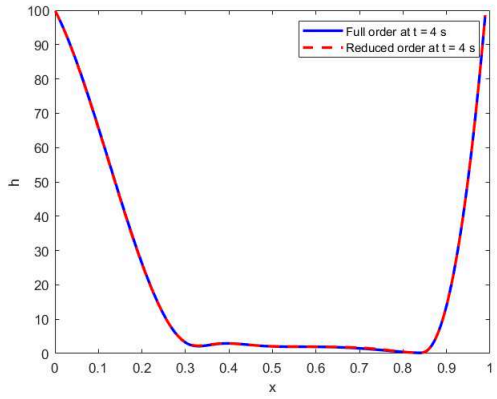

Fig. 12. Tear film thickness, full Vs reduced order systems at $t = 4$.

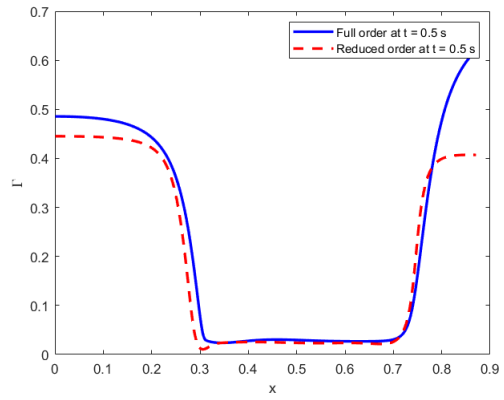

Fig. 13. Lipid concentration, full Vs reduced order systems at $t = 0.5$.

the film thickness and lipid concentration of tears proposed in [7] as are solved using a cell-edge-cell-center point finite difference scheme. The numerical snapshots are used to derive reduced order POD-based models for the film tickness and lipid concentration. A Galerkin model for the temporal coefficients is obtained by conducting Galerkin projections on the POD modes. The latter is solved to obtain the temporal coefficients and thus the reduced order solutions that are compared with the full order numerical solutions with favorable results. Future work includes the use of the reduced order models as a control basis for smart tears with a surfactant that can modify the surface tension to prevent tear film breakup. Other reduced order such as cluster POD [17] and Isolable coordinates [22] will be explored as improved model reduction techniques alternatives to POD.

ACKNOWLEDGMENT

This work was supported in part by the National Science Foundation under grant No CMMI-1933583, and in part by the NSF grant No DMS-2012634.

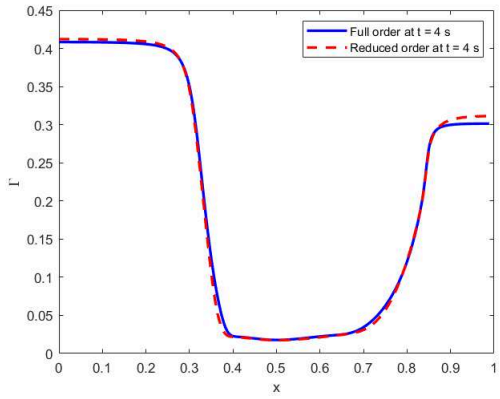

Fig. 14. Lipid concentration, full Vs reduced order systems at $t = 4$.

APPENDICES

A. Numerical Method

In this appendix we give some details of the numerical method employed for solving the system of PDEs. The spacial domain is $\Omega = [0,1]$. We use a finite difference method with a uniform grid spacing $\delta := 1/N$, where N is a positive integer. We set $p_i := (i-1/2)\delta$. The cell-edge and cell-center point sets are defined, respectively, as

$$E := \{p_{i+1/2} \mid i = 0,\ldots,N\} \quad \text{and} \quad C := \{p_i \mid i = 1,\ldots,N\}.$$

To handle boundary conditions, we add the two cell-center ghost points $p_0 = -\delta/2$ and $p_{N+1} = 1+\delta/2$. The larger cell-center point set that includes the ghost cells is denoted C_g:

$$C_g := \{p_i \mid i = 0,\ldots,N+1\} = C \cup \{p_0, p_{N+1}\}.$$

Next, we introduce spaces of cell-edge and cell-center grid functions, respectively, via

$$\mathcal{E} := \{f : E \to \mathbb{R}\}, \quad \mathcal{C} := \{u : C \to \mathbb{R}\}, \quad \mathcal{C}_g := \{u : C_g \to \mathbb{R}\}.$$

We define the edge-to-center difference and averaging operators $d, a : \mathcal{E} \to \mathcal{C}$ point-wise via

$$df_i := \frac{f_{i+1/2} - f_{i-1/2}}{\delta}, \quad af_i := \frac{f_{i+1/2} + f_{i-1/2}}{2}.$$

The center-to-edge difference and averaging operators $D, A : \mathcal{C}_g \to \mathcal{E}$ are defined point-wise via

$$Du_{i+1/2} := \frac{u_{i+1} - u_i}{\delta}, \quad Au_{i+1/2} := \frac{u_{i+1} + u_i}{2}.$$

The second difference operator $\Delta_\delta : \mathcal{C}_g \to \mathcal{C}$ is the composition of d and D and is defined as

$$\Delta_\delta u_i := d(Du)_i = \frac{u_{i+1} - 2u_i + u_{i-1}}{\delta^2}.$$

The solution $h(x,t)$ is approximated by the cell-center grid function $h_\delta(t)$, and, similarly, $\Gamma(x,t)$ is approximated by the cell-center grid function $\Gamma_\delta(t)$. We introduce the cell-center grid function $q_\delta(t)$ as an approximation of h_{xx}. Specifically,

$$q_\delta(t) := \Delta_\delta h_\delta(t).$$

The second-order-in-space semi-discretized equations are

$$\frac{dh_\delta}{dt} = x\frac{L_t}{L}a(Dh_\delta) - \frac{CH^2}{3L}d\left(A(h_\delta^3)\left(\frac{H}{L^3}Dq_\delta - B\right)\right) + \frac{MH}{2L^2}d\left(A(h_\delta^2)D\Gamma_\delta\right),$$

$$\frac{d\Gamma_\delta}{dt} = x\frac{L_t}{L}a(D\Gamma_\delta) - \frac{CH^2}{2L}d\left(A(h_\delta^2\Gamma_\delta)\left(\frac{H}{L^3}Dq_\delta - B\right)\right) + \frac{MH}{2L^2}d\left(A(h_\delta\Gamma_\delta)D\Gamma_\delta\right),$$

where $x \in \mathcal{C}$ is the cell-center grid function satisfying $x_i = p_i$. The boundary conditions are handled as follows:

$$Ah_\delta(t)_{1/2} = 1, \qquad Ah_\delta(t)_{N+1/2} = 1,$$

$$Dq_\delta(t)_{1/2} = \frac{L^3B}{H}, \qquad Dq_\delta(t)_{N+1/2} = \frac{L^3}{H}\left(B + 6\frac{L_t}{CH^2}\right),$$

$$D\Gamma_\delta(t)_{1/2} = 0, \qquad D\Gamma_\delta(t)_{N+1/2} = 2\frac{LL_t}{MH}.$$

The resulting coupled system of ODEs is integrated in time using a stiff ODE solver in Matlab.

B. Galerkin Projection

Galerkin projection is done by performing the inner product defined in (12) for both sides of (3) and (4) with the j^{th} basis functions $\phi_j^h(x)$ and $\phi_j^\Gamma(x)$. Due to the orthogonality of POD basis, the left hand sides of (3) and (4) become:

$$\int_\Omega h_t(x,t)\phi_j^h(x)dx = \alpha_{t_j}^h(t)$$

$$\int_\Omega \Gamma_t(x,t)\phi_j^\Gamma(x)dx = \alpha_{t_j}^\Gamma(t)$$

Integrating the first term in the right hand sides yields:

$$\int_\Omega \left(h^2\Gamma_x\right)_x \phi_j^h dx = h^2\Gamma_x\phi_j^h\Big|_{\partial\Omega} - \int_\Omega h^2\Gamma_x\phi_{x_j}^h dx$$

$$\int_\Omega \left(h\Gamma\Gamma_x\right)_x \phi_j^\Gamma dx = h\Gamma\Gamma_x\phi_j^\Gamma\Big|_{\partial\Omega} - \int_\Omega h\Gamma\Gamma_x\phi_{x_j}^\Gamma dx$$

Integrating the second term in the right hand sides yields:

$$\int_\Omega \left(h^3(\frac{H}{L^3}h_{xxx} - B)\right)_x \phi_j^h dx = h^3(\frac{H}{L^3}h_{xxx} - B)\phi_j^h\Big|_{\partial\Omega} - \int_\Omega h^3(\frac{H}{L^3}h_{xxx} - B)\phi_{x_j}^h dx$$

$$\int_\Omega \left(h^2\Gamma(\frac{H}{L^3}h_{xxx} - B)\right)_x \phi_j^\Gamma dx = h^2\Gamma(\frac{H}{L^3}h_{xxx} - B)\phi_j^\Gamma\Big|_{\partial\Omega} - \int_\Omega h^2\Gamma(\frac{H}{L^3}h_{xxx} - B)\phi_{x_j}^\Gamma dx$$

Integrating the third term in the right hand sides yields:

$$\int_\Omega xh_x\phi_j^h dx = xh\phi_j^h\Big|_{\partial\Omega} - \int_\Omega h(\phi_j^h + x\phi_{x_j}^h)dx$$

$$\int_\Omega x\Gamma_x\phi_j^\Gamma dx = x\Gamma\phi_j^\Gamma\Big|_{\partial\Omega} - \int_\Omega \Gamma(\phi_j^\Gamma + x\phi_{x_j}^\Gamma)dx$$

REFERENCES

[1] F. J. Holly and M. A. Lemp, "Tear physiology and dry eyes," *Surv Ophthalmol*, vol. 22, pp. 69 – 87, 1977.

[2] M. Lemp, C. Baudoin, J. Baum, M. Dogru, G. Foulks, and et al, "The definition and classification of dry eye disease: Report of the definition and classification subcommittee of the international dry eye workshop (2007)," *Ocul Surf.*, vol. 5, no. 2, pp. 75–92, 2007.

[3] W. K. I. T. M. A. Heidari M, Noorizadeh F, "Dry eye disease: Emerging approaches to disease analysis and therapy." *J Clin Med.*, vol. 8, p. 1439, 9 2019.

[4] A. AA, "Changes in blink rate and ocular symptoms during different reading tasks," *Clin Optom*, vol. 9, pp. 133–138, 9 2017.

[5] "Tearfilm exchange, just one more reason, online article," https://www.eyedolatryblog.com/2015/10/tear-film-exchange-just-one-more-reason.html, accessed: 09-27-2020.

[6] M. Bruna and C. J. W. Breward, "The influence of non-polar lipids on tear film dynamics," *J. Fluid Mech.*, vol. 746, pp. 565–605, 5 2014.

[7] E. Aydemir, C. Breward, and T. Witelski, "The effect of polar lipids on tear film dynamics," *Bulletin of mathematical biology*, vol. 73, no. 6, pp. 1171–1201, 2011.

[8] R. J. Braun and A. D. Fitt, "Modeling the drainage of the precorneal tear film after a blink," *Math. Med. Biol.*, vol. 20, pp. 1–28, 2003.

[9] R. J. Braun, "Dynamics of the tear film," *Annu Rev Fluid Mech*, vol. 44, pp. 267–297, 2012.

[10] A. Sharma and E. Ruckenstein, "An analytical nonlinear theory of thin film rupture and its application to wetting films," *J. Colloid Interface Sci*, vol. 113, no. 2, pp. 456–479, 1986.

[11] ——, "The role of lipid abnormalities, aqueous and mucus deficiencies in the tear film breakup, and implications for tear substitutes and contact lens tolerance," *J. Colloid Interface Sci*, vol. 111, no. 1, pp. 8–34, 1986.

[12] M. B. Jones, D. L. S. McElwain, G. R. Fulford, M. J. Collins, and A. P. Roberts, "The effect of the lipid layer on tear film behavior," *Bull. Math. Biol.*, vol. 68, pp. 1355–1381, 2006.

[13] R. J. Braun and P. E. King-Smith, "Model problems for the tear film in a blink cycle: Single equation models," *J. Fluid Mech.*, vol. 586, pp. 465–490, 2007.

[14] M. Allouche, H. A. Abderrahmane, S. M. Djouadi, and K. Mansouri, "Influence of curvature on tear film dynamics," *European Journal of Mechanics - B/Fluids*, vol. 66, pp. 81 – 91, 2017. [Online]. Available: http://www.sciencedirect.com/science/article/pii/S0997754616300991

[15] R. E. Berger and S. Corrsin, "A surface tension gradient mechanism for driving the pre-corneal tear film after a blink," *J of Biomech*, vol. 7, no. 3, pp. 225 – 238, 1974.

[16] P. Holmes, J. Lumley, and G. Berkooz, *Turbulence, Coherent Structures, Dynamical Systems and Symmetry*, ser. Cambridge Monographs on Mechanics. Cambridge University Press, 1998. [Online]. Available: https://books.google.com/books?id=7vS1nPYDe10C

[17] S. Sahyoun and S. M. Djouadi, "Control of nonlinear {PDEs} based on space vectors clustering reduced order systems," *{IFAC} Proceedings Volumes*, vol. 47, no. 3, pp. 5181 – 5186, 2014, 19th {IFAC} World Congress. [Online]. Available: http://www.sciencedirect.com/science/article/pii/S1474667016424183

[18] S. Sahyoun, J. Dong, and S. M. Djouadi, "Reduced order modeling for fluid flows subject to quadratic type nonlinearities," in *2012 IEEE 51st IEEE Conference on Decision and Control (CDC)*. IEEE, 2012, pp. 961–966.

[19] M. Jones, D. McElwain, G. Fulford, M. Collins, and A. Roberts, "The effect of the lipid layer on tear film behaviour," *Bulletin of mathematical biology*, vol. 68, no. 6, pp. 1355–1381, 2006.

[20] R. J. Braun and A. Fitt, "Modelling drainage of the precorneal tear film after a blink," *Mathematical Medicine and Biology*, vol. 20, no. 1, pp. 1–28, 2003.

[21] A. Heryudono, R. Braun, T. Driscoll, K. Maki, L. Cook, and P. King-Smith, "Single-equation models for the tear film in a blink cycle: realistic lid motion," *Mathematical medicine and biology: a journal of the IMA*, vol. 24, no. 4, pp. 347–377, 2007.

[22] D. Wilson and S. Djouadi, "Adaptive isostable reduction of nonlinear pdes with time varying parameters," *IEEE Control Letters*, vol. 5, no. 1, pp. 187–192, 2021.